Journal of Power Sources 199 (2012) 214–219

Contents lists available at SciVerse ScienceDirect

Journal of Power Sources

journal homepage: www.elsevier.com/locate/jpowsour

Synthesis and electrochemical characterization of multi-cations doped spinel $LiMn_2O_4$ used for lithium ion batteries

Lilong Xiong[a,b], Youlong Xu[a,*], Tao Tao[a], John B. Goodenough[b,**]

[a] Electronic Materials Research Laboratory, Key Laboratory of the Ministry of Education, Xi'an Jiaotong University, Xi'an 710049, PR China
[b] Texas Materials Institute, University of Texas at Austin, Austin, TX 78712, United States

ARTICLE INFO

Article history:
Received 30 July 2011
Received in revised form
12 September 2011
Accepted 21 September 2011
Available online 14 October 2011

Keywords:
Manganese spinel
Multi-cations doping
Capacity retention
Rate performance
Lithium-ion batteries

ABSTRACT

Homogeneous substitution of Cu(II), Al(III) and Ti(IV) for Mn in the spinel $Li[Mn_2]O_4$ is synthesized by lactic-acid assisted Pechini method. Galvanostatic charge–discharge between 3.5 and 4.3 V (versus Li^+/Li) at C/2 rate shows that the multi-cations doped spinel exhibits initial discharge capacity of 134 mAh g^{-1} with a 97% capacity retention after 400 cycles at room temperature. When cycling at 55 °C, the doped sample shows 91% capacity retention after 50 cycles compared to 70% retention for the undoped sample. As the charge–discharge rate increases to 12C, the doped sample delivers capacity of 111 mAh g^{-1}, which is much higher than that of the undoped sample of only 84 mAh g^{-1}. Moreover, as the charge–discharge rate returns from 12C to C/2, the discharge capacity of the doped electrode recovers nearly completely while the undoped sample lost more than 7% of its capacity.

1. Introduction

The $[B_2]O_4$ framework of the cubic $A[B_2]O_4$ spinel is first demonstrated by Thackeray et al. to be a viable Li-insertion host for a rechargeable electrode of a Li-ion battery in $Li_x[Mn_2]O_4$ [1,2]. A change in discharge voltage from 4 V to 3 V on increasing x at $x = 1.0$, where Li^+ ions change position from tetrahedral to octahedral sites of the interstitial space of the spinel framework, has concentrated attention on the 4 V region ($0 < x < 1$) of $Li_x[Mn_2]O_4$. However, during charge and discharge, the Li^+ ion distribution within the host is not uniform and the host $[Mn_2]O_4$ array is plagued by capacity loss, particularly at elevated temperature, associated with Mn dissolution as a result of surface disproportionation reaction $2Mn^{3+} = Mn^{2+} + Mn^{4+}$. The Mn dissolution is aggravated by volume change and phase separation associated with cooperative Jahn-Teller orbital ordering on Mn^{3+} ions in region with $x \approx 1$ as well as by Li^+ ion ordering near $x = 0.5$. Shin and Manthiram [3,4] have summarized this problem and shown that by introducing Li^+ and M^{2+} ions into the host framework so as to reduce the difference in the volume of the two cubic phases appearing in the interval $0 < x < 0.5$ as well as the Mn^{3+} ion concentration, the Mn dissolution can be sharply suppressed.

Thirunakaran et al. [5] have reported that doping with trivalent and divalent cations can be effective in suppressing the capacity fade. Substitution of Ti for Mn has also been shown to slow Mn dissolution by increasing the stability of the spinel framework [6–8]. We report here an investigation of the effect of doping the $[Mn_2]O_4$ host framework with three cations of different valence: Cu(II), Al(III) and Ti(IV), trying to find a cathode material with high capacity retention as well as high discharge capacity. We have used a Pechini synthesis process assisted by lactic acid to obtain a homogeneous distribution of the three dopants.

2. Experimental

2.1. Materials and reagents

The following materials and reagents were used: tetra-n-butyl titanate (98%, Tianjin Chemical Industry, Tianjin, China), lactic acid (80–90%, Tianjin Chemical Industry, China), lithium nitrate (99%, Shanghai Chemical Industry, Shanghai, China), manganese nitrate (99%, Shanghai Chemical Industry, Shanghai, China), copper nitrate (99%, Shanghai Chemical Industry, Shanghai, China), aluminum nitrate (99%, Shanghai Chemical Industry, Shanghai, China), citric acid (99.5%, Tianjin Chemical Industry), and ethylene glycol (99%, Tianjin Chemical Industry).

* Corresponding author. Tel.: +86 29 82665161; fax: +86 29 82665161.
** Corresponding author.
E-mail addresses: ylxuxjtu@mail.xjtu.edu.cn (Y. Xu), jgoodenough@mail.utexas.edu (J.B. Goodenough).

0378-7753/$ – see front matter © 2011 Elsevier B.V. All rights reserved.
doi:10.1016/j.jpowsour.2011.09.062

2.2. Synthesis of undoped and multi-cations doped spinel

The doped spinel $LiMn_2O_4$ powder was prepared by lactic-acid assisted Pechini method. First, tetra-n-butyl titanate was chelated with lactic acid to form a stable titanate solution [9], and then lithium nitrate, manganese nitrate, copper nitrate and aluminum nitrate dissolved with the titanium solution in a 1:4 molar mixture of citric acid and ethylene glycol. The molar ratio of the Cu:Al:Ti:Mn was 0.02:0.02:0.02:1.94 for the doped sample. After strong stirring at 90 °C for 1 h, the solution was heated at 140 °C to induce esterification [10]. The viscosity of the solution gradually increased and its colour turned into dark. The viscous solution was then dried at 180 °C to form dry gel. The gel was precalcined at 400 °C for 6 h in the air then grinded by ball milling for 2 h; finally, the powder was calcined at 800 °C for 12 h and furnace-cooled to room temperature to get the doped spinel material. The undoped $LiMn_2O_4$ was synthesized by the same method without adding the doping materials.

2.3. Characterizations and electrochemical measurements

To examine the heat and weight changes during the calcination process, thermal behavior was studied by thermogravimetric-differential scanning calorimetry (TG-DSC, Netzsch STA 449C). The dry gel was heated at a rate of 10 °C min^{-1} from 35 to 850 °C under an air flow.

The X-ray diffraction (XRD) pattern was recorded at room temperature using a PANalytical, X'Pert PRO X diffractometer equipped with a Cu-Kα radiation (l = 0.15406 nm) by step scanning in the 2θ range of 10–80°.

The morphology of the prepared powder was determined by scanning electron microscope (SEM, JSM-7000F, JEOL). The chemical composition of the spinel materials was examined by energy dispersive X-ray spectrometry analysis (EDS).

Electrochemical testing was performed in 2016 coin type cells with lithium foil as the negative electrode. The positive electrodes were prepared by mixing the active powder with carbon black and polyvinylidene fluoride in N-methyl-2-pyrrolidone. The electrochemical test cells were assembled in Mikrouna Super glove box under a dry argon atmosphere. Electrolyte was 1 M $LiPF_6$ dissolved in ethylene carbonate:diethyl carbonate:ethyl methyl carbonate in a 1:1:1 volume ratio.

The Mn dissolution in electrolyte was measured. Each sample (0.5 g) was immersed in 20 mL electrolyte for two weeks at 55 °C. Inductively coupled plasma-atomic emission spectrometer (ICP-AES) was employed to measure the amount of the dissolution.

Charge–discharge characteristics were performed galvanostatically in a cut-off voltage limit of 4.3–3.5 V (versus Li^+/Li) by the Arbin Battery Test System. The electrochemical impedance (EIS) was conducted in a frequency range from 100 kHz to 10 mHz, and the perturbation amplitude was controlled at 5 mV. Prior to EIS measurements, the potential of the electrode was set to 4.1 V and held for 1 h. Then, the Li^+ concentration in the spinel was considered to have reached the equilibrium state.

3. Results and discussion

Fig. 1 shows the TG-DSC curves for the undoped and doped spinel precursor prepared by Pechini method. For the undoped sample, as seen in Fig. 1(a), there are four distinguishable transformation enthalpies, corresponding to weight losses observed in TG curves. The observed weight loss between 80 and 180 °C along with endothermic peak is attributed to the removal of adsorbed water and ethylene glycol. As the temperature increases, three exothermic transformations start to appear, which is due

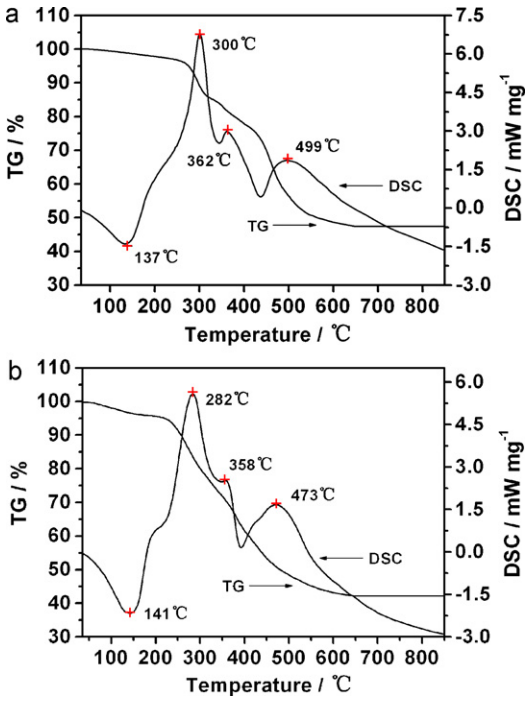

Fig. 1. TG-DSC curves of the precursor: (a) undoped spinel and (b) doped spinel.

to the combustion/pyrolysis of the organic component, and the formation of spinel phase. The doped sample exhibits similar TG-DSC curves, just as seen in Fig. 1(b). However, the TG curve for doped sample is smooth in the range from 240 to 530 °C; and for the undoped sample, the curve exhibits several inflection point. The difference is mainly due to the combustion/pyrolysis of the tetra-n-butyl titanate and lactic acid in the doped sample.

Fig. 2 shows the XRD patterns of the undoped and doped samples. The diffraction peaks of the samples are identified as a single-phase in the cubic spinel Fd-3m space group. It is noted that the (2 2 0) peak which arises only from the diffraction of tetrahedral sites (8a) lies at $2\theta \approx 30.7$ [11], cannot be observed in the patterns. The fact indicates that the tetrahedral sites (8a) are only occupied by lithium atoms which give undetectable (2 2 0) signals due to their very low X-ray scattering ability and the substituting metal ions only occupy octahedral (16d) sites to substitute manganese ions. It is reported that the doping could increase the peak intensity ratio

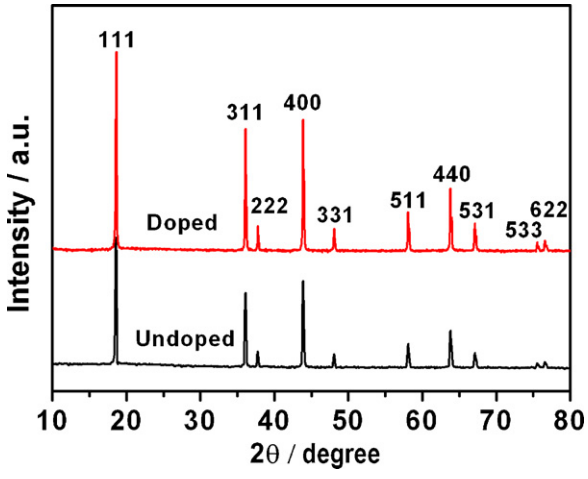

Fig. 2. The XRD patterns of the samples.

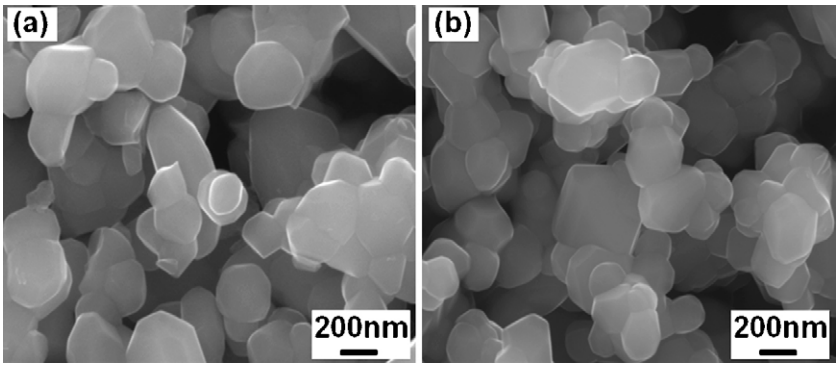

Fig. 3. SEM micrographs of the samples: (a) undoped sample and (b) doped sample.

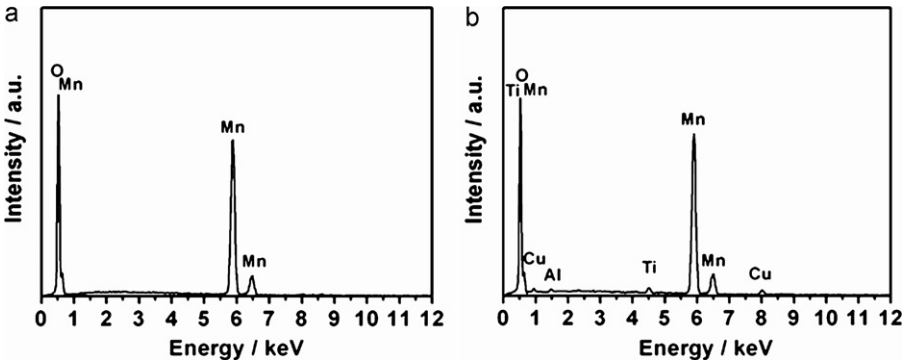

Fig. 4. EDS profiles of the samples: (a) undoped sample and (b) doped sample.

of (3 1 1)/(4 0 0) and the spinel shows good cycle performance when the ratio is at the range of 0.96–1.1 [12]. The ratio of (3 1 1)/(4 0 0) in our experiment increases from 0.89 for undoped sample to 0.96 for the doped sample, suggesting the multi-cations doped spinel would exhibit better electrochemical performance than that of undoped spinel.

Fig. 3(a) and (b) show the SEM micrographs of the undoped sample and doped sample respectively. Both the samples display octahedral morphology. However, the surface morphology of the doped sample shows more regular cubic shapes indicating that the doped sample has higher crystallinity than the undoped sample. EDS analysis is shown in Fig. 4. The doping elements, copper,

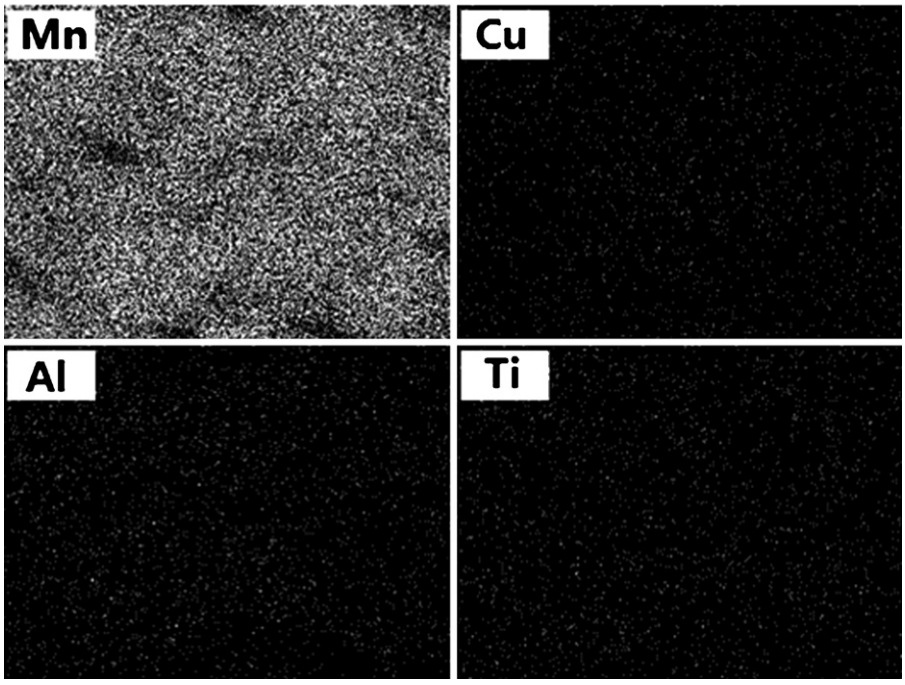

Fig. 5. SEM mappings of the Mn, Cu, Al, and Ti ions.

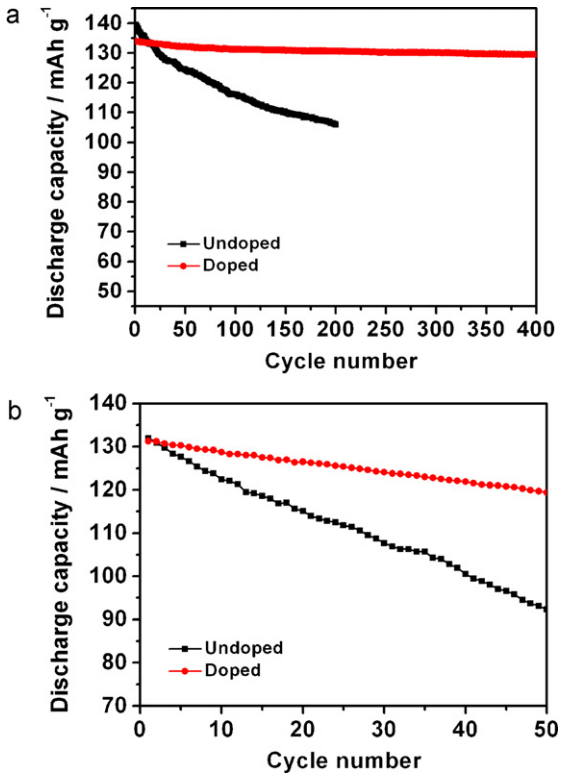

Fig. 6. The cycling performance of the samples: (a) at 25 °C and (b) at 55 °C.

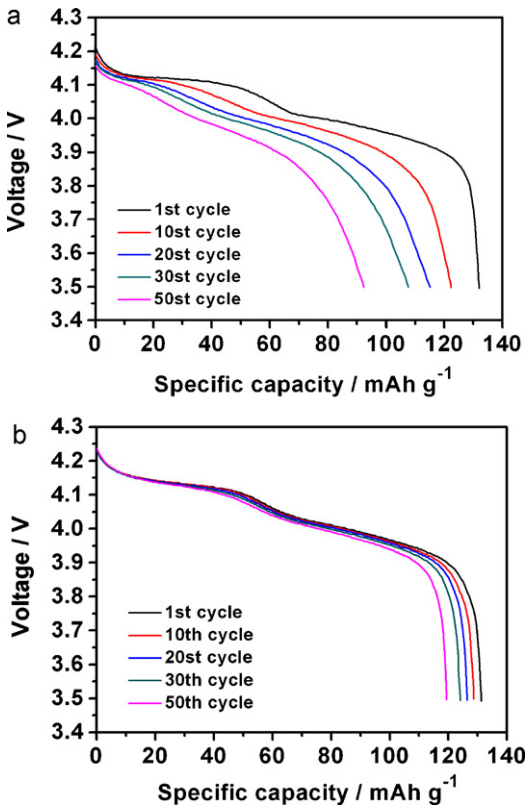

Fig. 7. The discharge curves of the samples cycling at 55 °C: (a) undoped sample and (b) doped sample.

aluminum and titanium could be clearly observed on the surface of the doped spinel.

For the metal ion doped materials, the chemical homogeneity is a key issue. SEM mappings of the Mn, Cu, Al, Ti are shown in Fig. 5 to evaluate the distribution of the doped ions in the particle. As seen in the figure, all the metal ions are well distributed. Due to the difference of the X-ray scattering factor, the strength of the mapping trace for the doping cations is slightly different. As for the Mn ion, the mapping trace is much stronger than that of the others mainly due to the content difference.

The charge–discharge characteristics are performed galvanostatically at a current rate of C/2. Fig. 6(a) shows the cycling performance of the samples at 25 °C. The undoped spinel delivers initial discharge capacity of 140 mAh g^{-1}; and after 200 cycles, the capacity decreases rapidly to 106 mAh g^{-1} with only 76% capacity retention. For the doped spinel, the initial capacity is 134 mAh g^{-1}; and it still delivers 130 mAh g^{-1} after 400 cycles with 97% capacity retention. The electrochemical performance of the multi-cations doped spinel material in our experiment is better than that of the dual-doped spinel [5,13] and the single-ion doped spinel [7,14]. The variation of discharge capacity as a function of cycle number for the undoped and doped samples cycling at 55 °C is given in Fig. 6(b). The undoped sample exhibits 70% capacity retention after 50 cycles; while at the same condition, the capacity retention ratio of the doped samples is 91%. The results of the galvanostatic charge–discharge indicate that the doping could effectively improve the cycling performance of the spinel $Li[Mn_2]O_4$.

The reason on the improvement of electrochemical performance of the spinel $Li[Mn_2]O_4$ by cationic substitution has been intensively studied [15–21]. It is reported that the metal-ion substitution could improve the stability of the spinel structure and suppress the Mn dissolution. Fig. 7 gives the discharge curves of the samples cycling at 55 °C. The undoped sample displays obvious voltage plateaus approximately at 4 V in its first cycle, and the discharge voltage plateaus are distorted gradually as cycling. For the doped sample, as seen in Fig. 7(b), the voltage step is less pronounced, and it exhibits consistent discharge curves during cycling. This indicates that the doped sample exhibits more stable spinel structure during charge–discharge process.

The Mn dissolution in electrolyte is carried out to investigate the effect of doping on suppressing the dissolution. By soaking the undoped and doped spinel powder respectively in electrolyte at 55 °C for two weeks, the Mn-dissolution content is determined by ICP-AES and the results are shown in Table 1. The doped sample exhibits much less dissolution content compared to the undoped sample. This suggests metal ions doping is an effective way to reducing the Mn dissolution.

While the multi-cations doped spinel exhibits greatly improved long-cycle life, it still shows relatively high rate performance. As shown in Fig. 8, the comparison of rate capability between the undoped and doped spinel at charge–discharge rates ranging from C/2 to 12C is evaluated. Due to the limited diffusion rate of the lithium ions in the spinel particles, both samples show decreased capacities at high rate charge–discharge cycles. The undoped spinel delivers only 84 mAh g^{-1} at 12C. However, the doped spinel could deliver 111 mAh g^{-1} at the same rate. Moreover, after 70 cycles, as the charge–discharge rates reduce from 12C to C/2, the discharge capacity of the doped spinel could be recovered nearly without capacity loss, but the undoped spinel shows more than 7% capacity fade of the 10th cycle at C/2 rate.

Table 1
The Mn dissolution of the samples.

Sample name	Mn dissolution (ppm)
Undoped	480 ± 2
Doped	67 ± 2

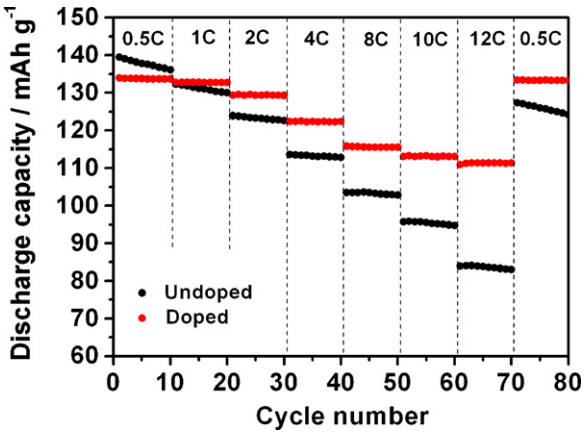

Fig. 8. The discharge capacity vs. cycle number at various charge–discharge rates of the samples.

The electrochemical impedance spectroscopy is measured to determine the kinetic parameters of the electrode process. The Nyquist plots for undoped spinel and doped spinel are shown in Fig. 9(a) and (b) respectively. The high-frequency semicircle results from the charge-transfer process, and the straight line is attributed to the diffusion of lithium ions in the spinel [22]. The EIS is fitted by the Zsimple analysis software (Bio-logic). The corresponding equivalent circuit is presented in Fig. 10. Where R_e is the ohmic electrolyte resistance, R_{ct} and C_{dl} are the charge transfer resistance and double-layer capacitance respectively, W is the finite length Warburg impedance, C_{int} is the reflection of intercalation capacitance [23]. The fitting results of the charge transfer resistance (R_{ct}) are shown in Table 2. Before cycles, the doped sample shows a little less charge-transfer resistance than the undoped sample. After

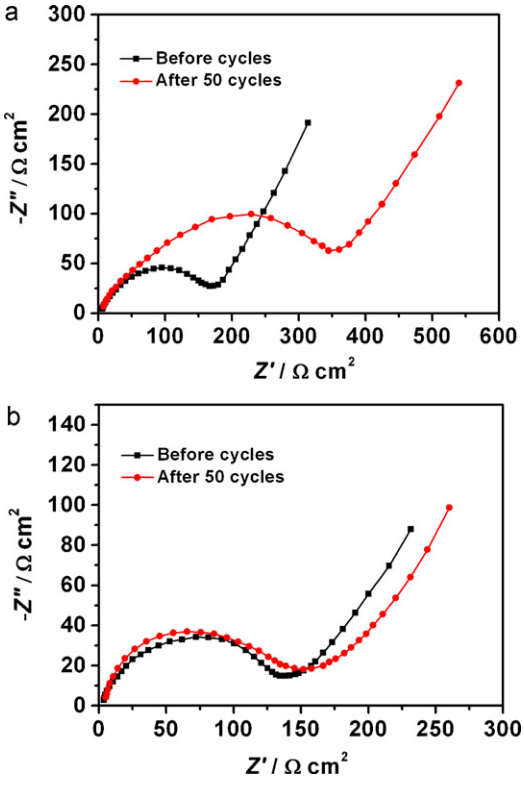

Fig. 9. The EIS of the samples before cycles and after 50 cycles at 55 °C: (a) undoped sample and (b) doped sample.

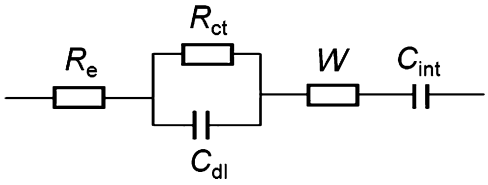

Fig. 10. The equivalent circuit for the EIS.

Table 2
The fitting values of the charge transfer resistance (R_{ct}) obtained from EIS.

Sample name	R_{ct} ($\Omega\,cm^2$) before cycles	R_{ct} ($\Omega\,cm^2$) after 50 cycles
Undoped	165.3 ± 0.3	362.7 ± 0.3
Doped	127.4 ± 0.3	138.6 ± 0.3

50 cycles at 55 °C, the charge-transfer resistance of the undoped sample electrode increases from 165.3 to 362.7 $\Omega\,cm^2$. However, for the doped spinel, the increase of the charge-transfer resistance is 11.2 $\Omega\,cm^2$, which is far lower than that of the undoped sample. This indicates that the metal-ions doping could effectively enhances the ion diffusion ability in the spinel, which makes the charge-transfer reaction easier.

4. Conclusion

Multi-cations (Cu, Al, Ti) doped spinel $Li[Mn_2]O_4$ has been synthesized by lactic acid assisted Pechini method. The X-ray diffraction analysis indicates the doped sample has well-defined single-phase in the cubic spinel with doping-ions occupying in the octahedral sites; and all the doping metal ions are homogeneously distributed in the spinel which confirmed by scanning electron microscopy mapping. The doped spinel delivers initial capacity of 134 mAh g^{-1} and exhibits 97% and 91% capacity retention after 400 cycles at 25 °C and 50 cycles at 55 °C respectively. The multi-cations doped spinel still exhibits relatively high rate capacity; and it shows 111 mAh g^{-1} even at 12C. The doped spinel exhibits much less Mn dissolution content compared to the undoped spinel. The electrochemical impedance analysis indicates that the multi-cations doping could effectively enhance the ion diffusion ability in the spinel.

References

[1] M.M. Thackeray, W.I.F. David, P.G. Bruce, J.B. Goodenough, Mater. Res. Bull. 18 (1983) 461–472.
[2] M.M. Thackeray, P.J. Johnson, L.A. de Picciotto, P.G. Bruce, J.B. Goodenough, Mater. Res. Bull. 19 (1984) 179–187.
[3] Y. Shin, A. Manthiram, Chem. Mater. 15 (2003) 2954–2961.
[4] Y.J. Shin, A. Manthiram, J. Electrochem. Soc. 151 (2004) A204–A208.
[5] R. Thirunakaran, A. Sivashanmugam, S. Gopukumar, R. Rajalakshmi, J. Power Sources 187 (2009) 565–574.
[6] Q.S. Tong, Y. Yang, J.C. Shi, J.M. Yan, L.Q. Zheng, J. Electrochem. Soc. 154 (2007) A656–A667.
[7] L.L. Xiong, Y.L. Xu, C. Zhang, Z.W. Zhang, J.B. Li, J. Solid State Electrochem. 15 (2011) 1263–1269.
[8] L.L. Xiong, Y.L. Xu, T. Tao, X.F. Du, J.B. Li, J. Mater. Chem. 21 (2011) 4937–4944.
[9] X.F. Du, Y.L. Xu, H.X. Ma, J. Wang, X.F. Li, J. Am. Ceram. Soc. 90 (2007) 1382–1385.
[10] W. Liu, G.C. Farrington, F. Chaput, B. Dunn, J. Electrochem. Soc. 143 (1996) 879–884.
[11] C. Bellitto, E.M. Bauer, G. Righini, M.A. Green, W.R. Branford, A. Antonini, M. Pasquali, J. Phys. Chem. Solids 65 (2004) 29–37.
[12] Y.-S. Lee, N. Kumada, M. Yoshio, J. Power Sources 96 (2001) 376–384.
[13] J.M. Amarilla, K. Petrov, F. Pico, G. Avdeev, J.M. Rojo, R.M. Rojas, J. Power Sources 191 (2009) 591–600.
[14] J.H. Lee, J.K. Hong, D.H. Jang, Y.K. Sun, S.M. Oh, J. Power Sources 89 (2000) 7–14.

[15] S.T. Myung, S. Komaba, N. Kumagai, J. Electrochem. Soc. 148 (2001) A482–A489.
[16] T. Tsuji, M. Nagao, Y. Yamamura, N. Tien Tai, Solid State Ionics 154–155 (2002) 381–386.
[17] Y. Ito, Y. Idemoto, Y. Tsunoda, N. Koura, J. Power Sources 119–121 (2003) 733–737.
[18] S.Q. Shi, D.S. Wang, S. Meng, L.Q. Chen, X.J. Huang, Phys. Rev. B 67 (2003) 115130.
[19] J.T. Son, H.G. Kim, Y.J. Park, Electrochim. Acta 50 (2004) 453–459.
[20] Y.J. Wei, L.Y. Yan, C.Z. Wang, X.G. Xu, F. Wu, G. Chen, J. Phys. Chem. B 108 (2004) 18547–18551.
[21] X.M. He, J.J. Li, Y. Cai, Y.W. Wang, J.R. Ying, C.Y. Jiang, C.R. Wan, J. Power Sources 150 (2005) 216–222.
[22] J. Xie, K. Kohno, T. Matsumura, N. Imanishi, A. Hirano, Y. Takeda, O. Yamamoto, Electrochim. Acta 54 (2008) 376–381.
[23] M.D. Levi, D. Aurbach, J. Phys. Chem. B 101 (1997) 4630–4640.